

# Bridging the Binding Sites: Dualsteric Ligands for the Cannabinoid 2 Receptor (CB<sub>2</sub>R)

Anna Tutov, Sophie A. M. Steinmüller, Yesid A. Ramírez, Christine E. Jack, Diego A. Rodríguez-Soacha, Christoph Sotriffer, James N. Hislop, and Michael Decker\*

The cannabinoid receptor subtype 2 (CB<sub>2</sub>R) is rapidly upregulated in neuroinflammatory processes and respective agonists have a high potential to combat several central nervous system disorders related to neuroinflammation and neurodegeneration. As a new strategy for ligand design, dualsteric binding is applied by chemically combining a positive allosteric modulator with an orthosteric ligand. The resulting two sets of potential dualsteric (or bitopic) ligands with different chain lengths of two to five methylene groups are evaluated in [<sup>3</sup>H]CP55940 binding studies to determine receptor affinity at CB<sub>1</sub>R and CB<sub>2</sub>R. Calcium mobilization, receptor endocytosis and BRET assays determine their efficacy and identify compounds of set B to act as agonists with efficacy higher than the reference compound in G protein mediated calcium signaling. Pharmacological evaluation and docking studies support the dualsteric nature of binding of the herein presented compounds.

## 1. Introduction

The cannabinoid receptor type 2 (CB<sub>2</sub>R) is a G protein-coupled receptor (GPCR) and is mostly expressed in peripheral organs, especially in cells associated with the immune system.<sup>[1]</sup> Among others, CB<sub>2</sub>R is a target of interest in Alzheimer's disease (AD) research, as it is overexpressed in neurodegenerative disorders.<sup>[2]</sup> One way to selectively activate the receptor of interest and to avoid undesirable side effects—caused by off-target binding—is to apply the dualsteric targeting strategy.<sup>[3]</sup> The heterobivalent ligands obtained by this approach consist of a covalently linked pair of an orthosteric and an allosteric ligand. Allosteric modulators are classified as either positive allosteric modulators (PAM) or negative allosteric modulators (NAM),


which either positively or negatively influence receptor response of an orthosteric ligand without causing receptor response by themselves—in contrast to allosteric agonists. Receptor modulation initiated by allosteric binding has many advantages over the more common orthosteric receptor activation, such as receptor subtype selectivity because of higher sequence divergence at allosteric binding sites. Through the resulting conformational changes in the receptor, allosteric modulators affect affinity and/or efficacy of bound orthosteric ligands and in some cases also promote stimulus bias.<sup>[4]</sup> But allosteric modulators rely on the presence of endogenous agonists, which is not always the case in progressing neurodegenerative disorders as AD, which goes in hand with loss of synapses and neurons in the cerebral cortex and certain subcortical regions.<sup>[5]</sup> While many dualsteric ligands (with remarkable properties at the receptor, such as various degrees of partial agonism,) are described for other GPCRs like the muscarinic receptors,<sup>[6]</sup> by now and to our knowledge, only two bitopic CB<sub>2</sub> ligands are reported in literature. In 2020, Morales et al. have presented a CB<sub>2</sub> homobivalent bitopic ligand, which links two identical orthosteric pharmacophores to a hybrid ligand.<sup>[7]</sup> Very recently, Gado et al. have presented the first dualsteric heterobivalent ligands, which combine the only synthetic positive allosteric modulator (1)—also described by Gado et al.<sup>[8]</sup>—and a structurally related orthosteric ligand (FM-6b, **Figure 1**).<sup>[9]</sup> The authors presented a set of eight heterobivalent ligands with different linker lengths which were pharmacologically evaluated. The most promising compound FD-22a showed anti-inflammatory activity in a human microglial cell inflammatory

A. Tutov, S. A. M. Steinmüller, Y. A. Ramírez, D. A. Rodríguez-Soacha, C. Sotriffer, M. Decker  
Pharmaceutical and Medicinal Chemistry, Institute of Pharmacy and Food Chemistry  
Julius Maximilian University Würzburg  
97074 Würzburg, Germany  
E-mail: michael.decker@uni-wuerzburg.de

Y. A. Ramírez  
Department of Pharmaceutical Sciences, Faculty of Natural Sciences  
Icesi University, Cali  
Valle del Cauca 760031, Colombia

Y. A. Ramírez  
Cannaflos – Gesellschaft für medizinisches Cannabis mbH  
50827 Köln, Germany

C. E. Jack, J. N. Hislop  
School of Medicine, Medical Sciences and Nutrition, Institute of Medical Sciences  
University of Aberdeen  
Aberdeen, Scotland AB25 2ZD, UK

 The ORCID identification number(s) for the author(s) of this article can be found under <https://doi.org/10.1002/adtp.202200260>

© 2023 The Authors. Advanced Therapeutics published by Wiley-VCH GmbH. This is an open access article under the terms of the Creative Commons Attribution-NonCommercial License, which permits use, distribution and reproduction in any medium, provided the original work is properly cited and is not used for commercial purposes.

DOI: 10.1002/adtp.202200260

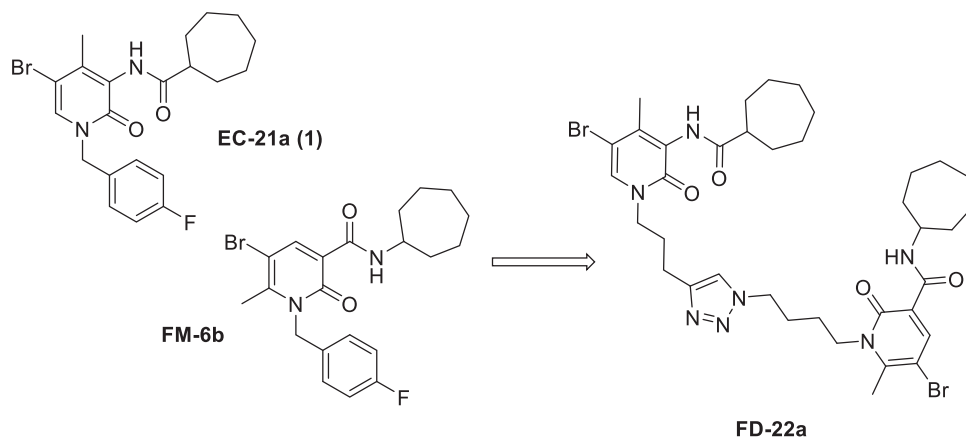


Figure 1. Dualsteric ligand FD-22a reported by Gado et al.<sup>[9]</sup>

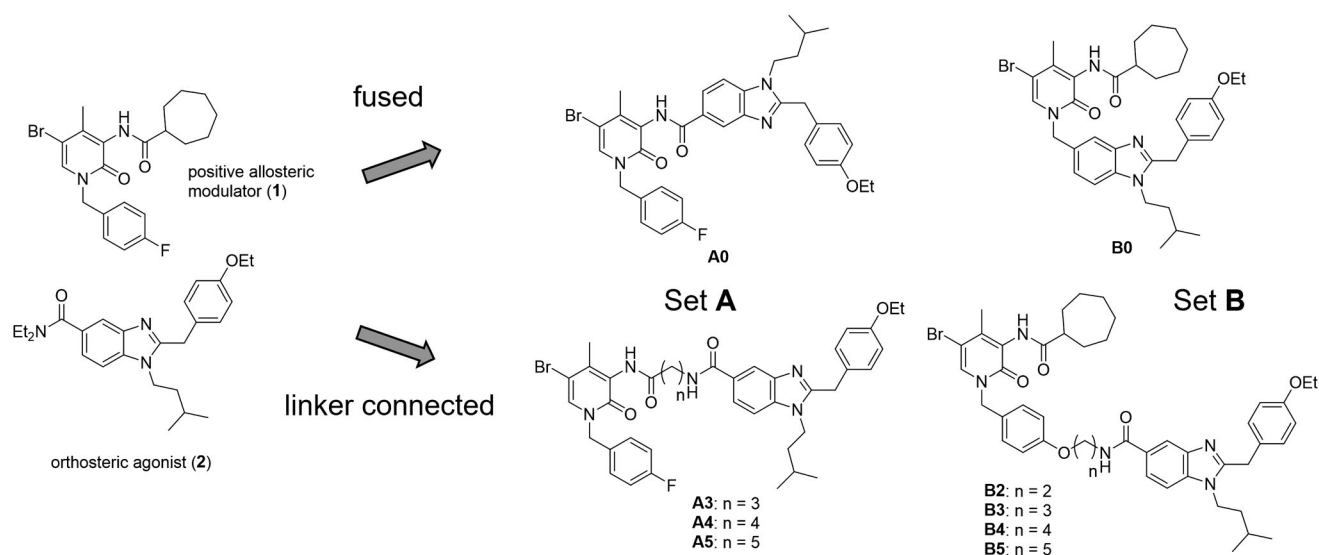


Figure 2. Design of set A and B compounds from allosteric modulator (1) and orthosteric agonist (2).

model and in an experimental mouse model of neuropathic pain, and the compound demonstrated antinociceptive activity in vivo.

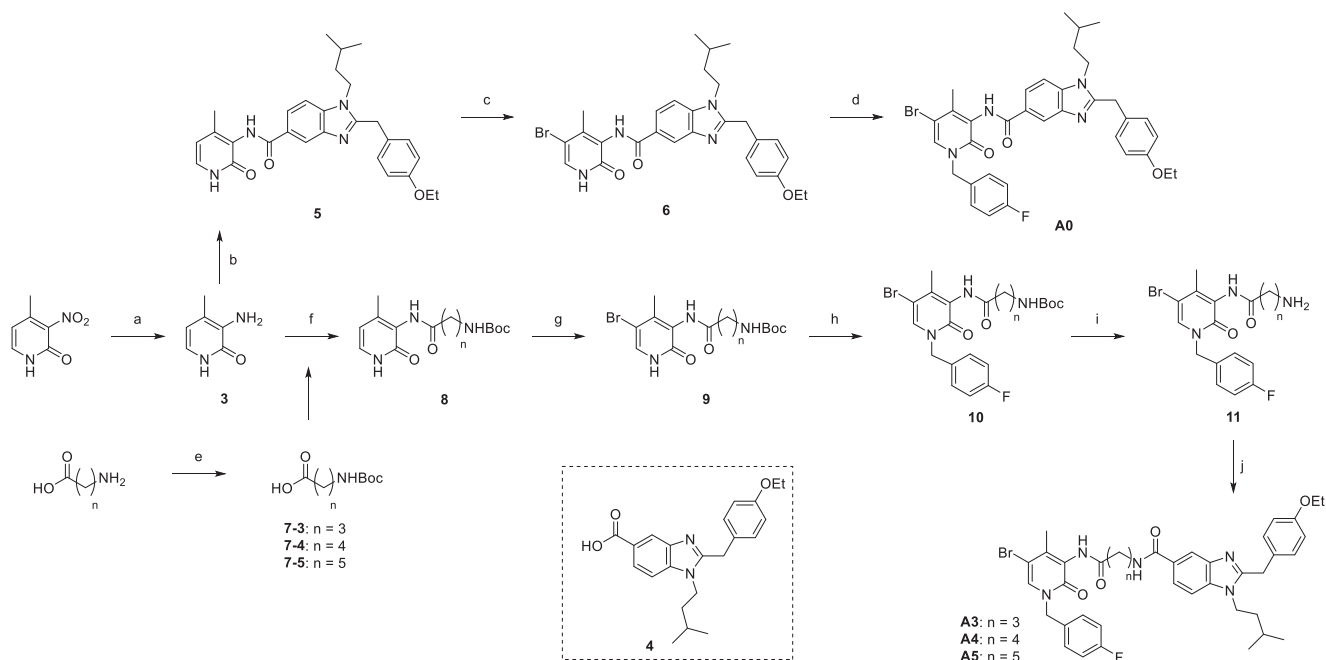
For our dualsteric targeting approach, we chose the positive allosteric modulator 1 and the CB<sub>2</sub> selective orthosteric agonist 2, first described by Astra Zeneca in 2008.<sup>[10]</sup> Due to probe dependence observed for allosteric modulation,<sup>[11]</sup> the pharmacological effects of bitopic compounds are hardly predictable. For the effective development of dualsteric ligands, it is important to evaluate the structure activity relationships (SARs) of both components. Analysis of the first SARs of the allosteric modulator showed that two positions of the molecule could be modified. Bromine in position 5 and methyl in position 4 are crucial, but the benzylic ring does tolerate modification.<sup>[8]</sup> We, therefore, chose to substitute the cycloheptyl ring (set A) or to elongate the benzyl ring (set B) for connection to the agonist part. We also designed fused ligands to get compounds with lower molecular weight and improved solubility (Figure 2). The resulting 12 molecules were evaluated by in vitro efficacy and affinity assays and showed novel and interesting pharmacological profiles.

## 2. Results and Discussion

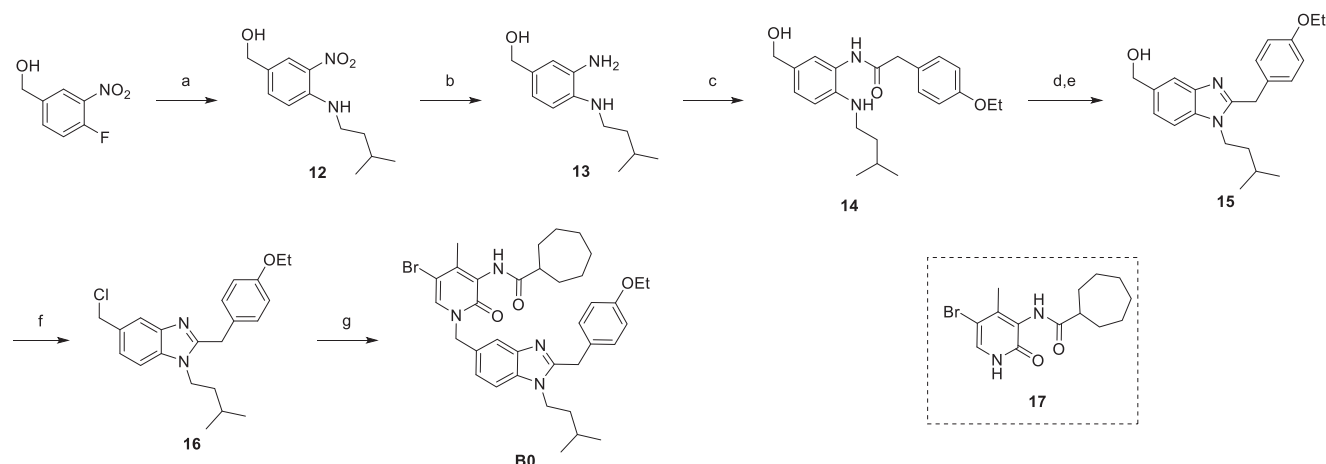
### 2.1. Chemistry

The two sets of compounds A and B were synthesized by distinct, non-linear synthetic routes. For the synthesis of set A ligands, the reaction sequence—amine reduction, amide coupling, bromination, and nucleophilic substitution—was adapted from synthesis of the respective allosteric modulator (1).<sup>[8]</sup>

The synthesis for set A ligands (fused and linked) shares the common intermediate amine 3 (Scheme 1). Ligand A0 was synthesized in 3 steps starting from 4-methyl-3-nitropyridin-2(1H)-one, which was first reduced with palladium on charcoal and hydrogen in MeOH. Fragment 4 was synthesized in 4 steps<sup>[12]</sup> and coupled with HATU and DIPEA in DMF, as with HBTU and Et<sub>3</sub>N the full conversion of the starting materials could not be achieved due to lower reactivity. After bromination with Br<sub>2</sub> in CHCl<sub>3</sub> for 10 min at room temperature and nucleophilic substitution with 4-fluorobenzyl chloride and K<sub>2</sub>CO<sub>3</sub> in DMF, compound A0



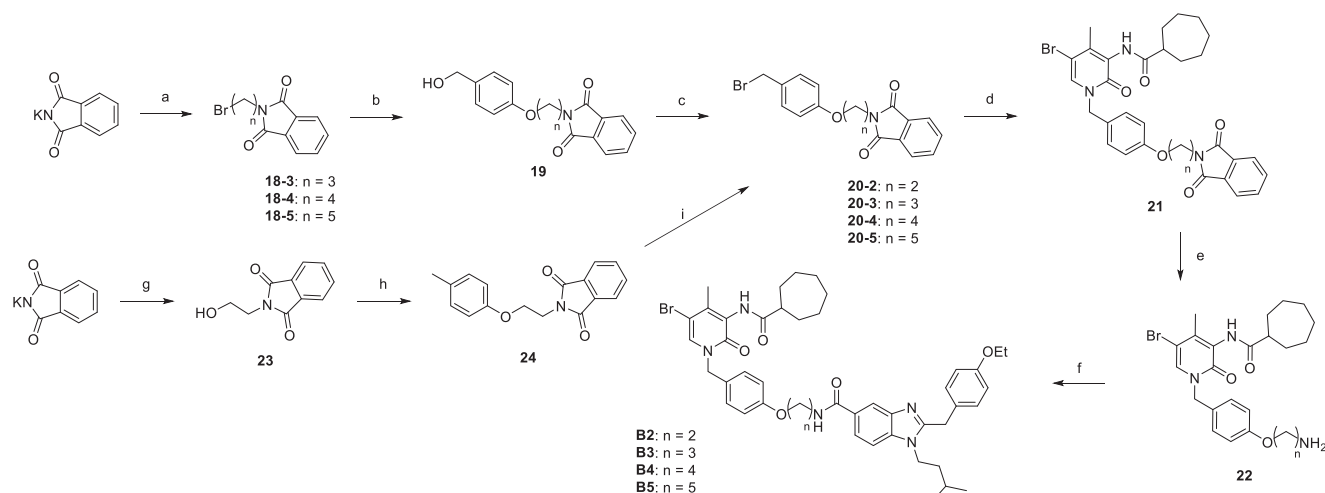
**Scheme 1.** Synthesis of set A ligands. Reagents and conditions: a) Pd/C, H<sub>2</sub>, MeOH, 12 h, r.t.; b) 4, HATU, DIPEA, DMF, 24 h, r.t.; c) Br<sub>2</sub>, CHCl<sub>3</sub>, 10 min, r.t.; d) 4-fluorobenzyl chloride, K<sub>2</sub>CO<sub>3</sub>, DMF, 18 h, 50 °C; e) Boc<sub>2</sub>O, NaOH, dioxan/H<sub>2</sub>O (2:1), 1 h, r.t.; f) *n*-(tert-butoxycarbonyl)amino acid, HBTU, Et<sub>3</sub>N, DMF, 24 h, r.t.; g) Br<sub>2</sub>, CHCl<sub>3</sub>, 2 h, r.t.; h) 4-fluorobenzyl chloride, K<sub>2</sub>CO<sub>3</sub>, DMF, 18 h, 70 °C; i) TFA/CH<sub>2</sub>Cl<sub>2</sub>, 20 min, r.t.; j) 4, HBTU, Et<sub>3</sub>N, DMF, 24 h, r.t.



**Scheme 2.** Synthesis of compound B0. Reagents and conditions: a) isoamylamine, Et<sub>3</sub>N, MeOH, 2 d, r.t.; b) Pd/C, H<sub>2</sub>, MeOH, 3 h, r.t.; c) 4-ethoxyphenylacetic acid, HBTU, Et<sub>3</sub>N, DMF, 24 h, r.t.; d) AcOH, 5 h, reflux; e) NaOH, THF, 3 h, reflux; f) SOCl<sub>2</sub>, CH<sub>2</sub>Cl<sub>2</sub>, 2 h, r.t.; g) 17, K<sub>2</sub>CO<sub>3</sub>, DMF, 18 h, 50 °C.

was obtained. Synthesis of A3–A5 derivatives started with Boc-protection of the corresponding amino acid (4-aminobutanoic to 6-aminohexanoic acid) using NaOH, followed by an HBTU amide coupling with amine 3. After bromination in position 5, molecule 9 was converted to compound 10 in a nucleophilic substitution reaction with 4-fluorobenzyl chloride and K<sub>2</sub>CO<sub>3</sub> in DMF. After deprotection with TFA in CH<sub>2</sub>Cl<sub>2</sub> for 20 min at room temperature, the free amine 11 was coupled with acid 4, HBTU and Et<sub>3</sub>N in DMF to obtain the target compounds A3–A5.

As described for set A, the fused compound B0 was prepared according to a different procedure than the linked ligands (Scheme 2). This approach was adapted from the reported synthesis of orthosteric ligand 2.<sup>[10]</sup> First, (4-fluoro-3-nitrophenyl)methanol reacted with iso-pentylamine and Et<sub>3</sub>N in MeOH to give compound 12, which was then reduced with palladium on charcoal and hydrogen for 3 h at room temperature. The resulting aniline 13 was converted to amide 14 by HBTU coupling with 4-ethoxyphenylacetic acid and Et<sub>3</sub>N in DMF. The ring closing reaction to compound 15 with acetic acid under reflux for



**Scheme 3.** Synthesis of set **B** ligands. Reagents and conditions: a)  $\alpha,\omega$ -dibromo-alkane, DMF, 18 h, r.t.; b) 4-(hydroxymethyl)phenol,  $K_2CO_3$ , DMF, 18 h, 70 °C; c)  $PPh_3$ ,  $CBr_4$ ,  $CH_2Cl_2$ , 2 h, 0 °C; d) **17**,  $K_2CO_3$ , DMF, 18 h, 70 °C; e) hydrazine hydrate, EtOH, 2 h, reflux; f) **4**, HBTU,  $Et_3N$ , DMF, 24 h, r.t.; g) 1-bromo-2-ethanol, DMF, 18 h, r.t.; h) *p*-cresol,  $PPh_3$ , DIAD, THF, 72 h, r.t.; i) NBS, DBPO,  $CHCl_3$ , 4 h, reflux.

5 h, first resulted in the undesired benzyl acetate, which had to be hydrolyzed with NaOH under reflux in an extra step. Alcohol **15** was converted to benzyl chloride **16** using thionyl chloride in  $CH_2Cl_2$ , which functioned as a leaving group in the last step, a nucleophilic substitution reaction with fragment **17** and  $K_2CO_3$ . The allosteric warhead **20** was synthesized in three steps according to the procedure described by Gado et al.<sup>[8]</sup>

To obtain ligands **B3–B5**, Gabriel amine synthesis was applied (**Scheme 3**). The required  $\alpha,\omega$ -dibromo-alkane (1,3-dibromopropane, 1,4-dibromobutane, or 1,5-dibromopentane, respectively) was reacted with potassium phthalimide in DMF for 18 h under vigorous stirring and with 4-(hydroxymethyl)phenol and  $K_2CO_3$  in DMF. The resulting benzyl alcohol **19** was converted to benzyl bromide **20** by an Appel reaction with  $PPh_3$  and  $CBr_4$  for 2 h at 0 °C and further reacted in a nucleophilic substitution reaction with fragment **17** and  $K_2CO_3$  in DMF. Phthalimide was then removed via hydrazinolysis in EtOH under reflux and the free amine **22** was coupled with benzimidazole acid **4** in an HBTU amide coupling to target compounds **B3–B5**. To get compound **B2** a different synthetic route was necessary since under the reaction conditions for step (b) described above, elimination of the bromine for compound **18** took place. Therefore, potassium phthalimide was instead reacted with 1-bromo-2-ethanol overnight in DMF. In the next step, a Mitsunobu reaction was performed, in which the hydroxy group of **24** reacted with the phenolic group of *p*-cresol using  $PPh_3$  and diisopropyl azodicarboxylate (DIAD) in THF at room temperature. Compound **25** was brominated in a radical reaction with NBS and DBPO in  $CHCl_3$  under reflux for 4 h to give intermediate **20–2**. The following steps toward compound **B2** were carried out in the same way as described above for ligands **B3–B5**.

To further explore the SARs of set **B**, ligand **B4** was chosen as a model compound to study the specific orientation of the linker relative to the allosteric modulator moiety by shifting the ether attached linker from *para* to *ortho* and *meta* positions. Thus, two isomers were synthesized—the *ortho* substituted **B4o** and the *meta* connected **B4m**. Syntheses of therein was carried as described

for **B4** (**Scheme 3**), only starting with the corresponding 2- or 3-(hydroxymethyl)phenol. Furthermore, in the course of this work, the cycloheptyl group has been identified as crucial for allosteric modulation by Gado et al. in further SAR studies.<sup>[13]</sup> To verify the allosteric binding of set **B** ligands, again compound **B4** as a model compound was modified by removing the cycloheptyl carboxyl from the allosteric head and introducing an acetyl moiety instead. For this, the altered allosteric warhead was prepared according to Scheme 1 by first reacting amine **3** with acetic anhydride, followed by bromination in position 5. The compound thus obtained was named **B4Ac** (**Figure 3**).

## 2.2. [<sup>3</sup>H]CP55940 Binding Assay

All compounds were tested for their binding affinities at CBRs in presence of [<sup>3</sup>H]CP55940, a high-affinity non-selective  $CB_1R$  and  $CB_2R$  agonist. The utilized membrane homogenates for  $CB_1R$  were prepared from brains of adult female rats, the respective  $CB_2R$  membranes were obtained from HEK293 cells overexpressing *hCB\_2R*. As control compounds for the binding experiments rimonabant ( $K_i = 56$  nM) was used for  $CB_1R$  and the orthosteric ligand **2** ( $K_i = 15$  nM) for  $CB_2R$ . We applied the non-selective CBR ligand CP55940 as a reference compound to provide a control for both systems ( $K_i$  ( $rCB_1R$ ) = 8.8 nM and  $K_i$  (*hCB\_2R*) = 13 nM). Regarding the  $CB_1R$  affinity, none of the tested compounds displaced the radioligand in a significant amount at 10  $\mu M$  (Table S1, Supporting Information). Most ligands bind with little to no affinity with the maximum value of [<sup>3</sup>H]CP55940 displacement for compound **B5** (23% at 10  $\mu M$ ).

In case of  $CB_2R$  binding, most of the target compounds showed moderate affinity in the 1-digit micromolar range (**Table 1**, **Figure 3A–C**) thereby validating excellent  $CB_2R$  subtype selectivity. Among set **A** (**Figure 3A**), compound **A3** with the shortest linker of three carbons showed incomplete displacement of the radioligand of 29% at 10  $\mu M$  and no dose-response curve could be recorded. The fused ligand **A0** enhanced binding of the

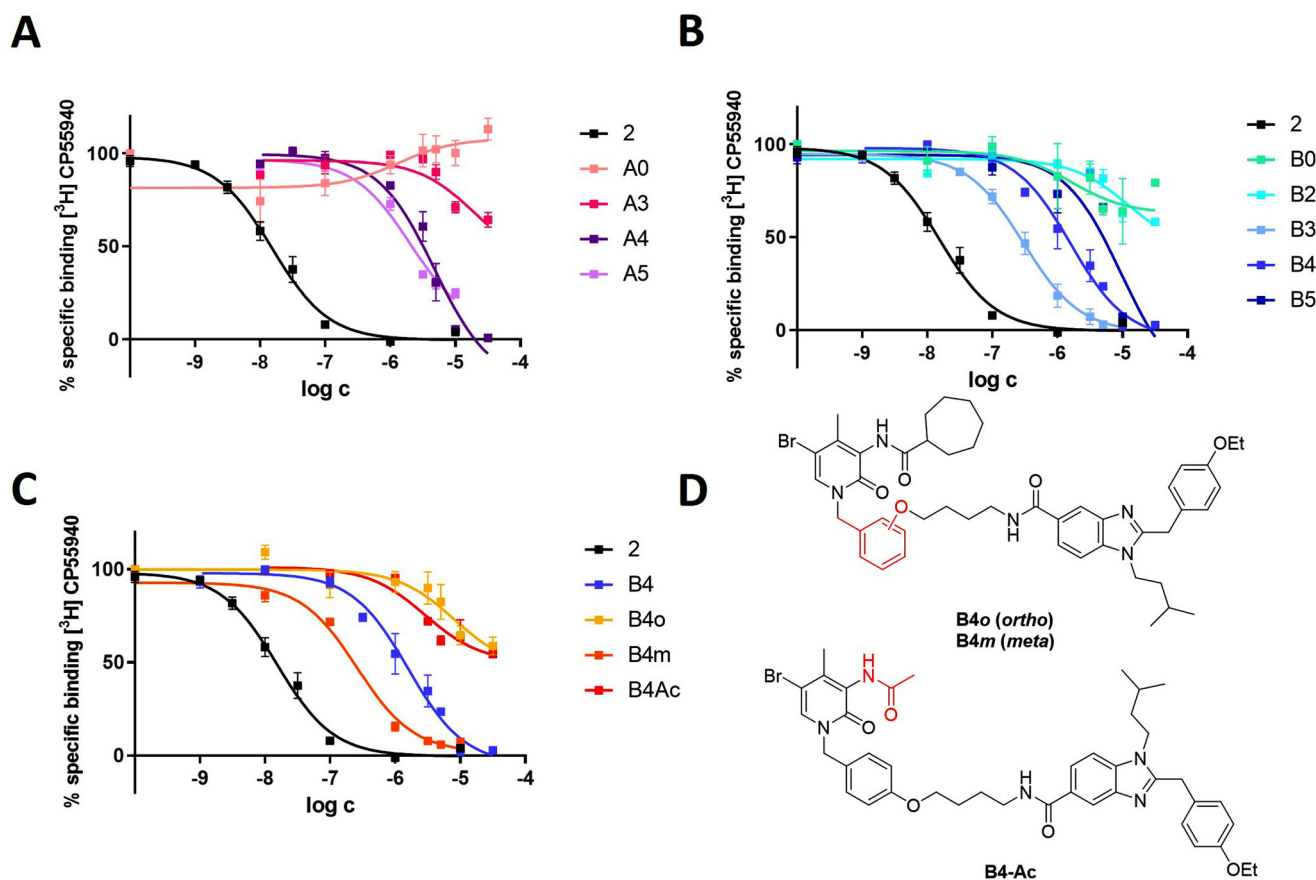


**Figure 3.** Radioligand binding data for all compounds to CB<sub>2</sub>R. Each data-point and error bar represent the average of at least three independent experiments by triplicate ± standard error of the mean (SEM); only two independent experiments by triplicate ± SEM were recorded for inactive compounds: A0, A3, B0, B2, and B4Ac, as a full sigmoidal curve could not be obtained due to a lack of binding to CB<sub>2</sub>R. A) Radioligand binding data for compounds of set A. B) Radioligand binding data for compounds of set B. C) Radioligand binding data for B4 derivatives. D) Structures of further derivatives of compound B4.

radioligand, which indicates that the behavior of the PAM is predominant in this molecule. Ligands A4 and A5 displaced the radioligand within a one-digit micromolar range ( $K_i = 4.6$  and  $2.0 \mu\text{M}$ , respectively), with the ligand bearing the longest carbon chain showing the best affinity within this set. These results indicate that for compounds of set A, a longer linker of five methylene groups is more beneficial than a short linker of three carbons. In addition, the fused-ligand approach did not work out for set A, since the corresponding molecule (A0) increases binding of the radioligand at higher concentrations but does not replace it.

For set B, a clear trend for binding the CB<sub>2</sub>R can be observed (Figure 3B). The affinity reaches a peak for ligand B3 ( $K_i = 290$  nM) and constantly decreases for B4 and B5 with  $1.5$  and  $9.1 \mu\text{M}$ , respectively. Based on the findings for compound B3 and with the intention to increase affinity, a ligand with a two-carbon chain (B2) was synthesized. Compound B2 showed a lower displacement of the radioligand for CB<sub>2</sub>R of only 37% at  $10 \mu\text{M}$  concentrations and no sigmoidal dose-response curve could be recorded. This is probably because the linker of two carbons is too short to bridge the orthosteric binding site and a nearby allosteric pocket. Compound B3 on the other hand turned out to have the optimal chain-length—for this set of compounds—of three methy-

lene groups. A longer linker of five carbons seems to be disadvantageous for binding to the CB<sub>2</sub>R, which is most likely due to the fact that a flexible long linker is forced into an unfavorable conformation and therefore leads to a loss in affinity both enthalpically and entropically.<sup>[14]</sup> The fused compound B0 drastically lost affinity on the receptor. Among the isomers of B4, the *ortho*-derivative (B4o) lost affinity for the CB<sub>2</sub> receptor by displacing the radioligand by 36% at the highest concentration only. The *meta* derivative B4m on the other hand, shows much improved affinity ( $K_i = 250$  nM) in comparison to B4 ( $1.5 \mu\text{M}$ ). With this, ligand B4m has a comparable affinity to compound B3 ( $K_i = 290$  nM), which suggests that shifting the aryl ether bridge from *para* (B4) to *meta* (B4m) affects the molecule's position inside the receptor and leads to comparable binding as for a linker with three methylene groups (B3). Last, removal of the cycloheptyl group from the allosteric part of the potential dualsteric ligands (B4Ac), as expected leads to an affinity drop and incomplete displacement of the radioligand to an amount of only 36% at  $10 \mu\text{M}$ . This supports the ability of set B compounds to also bind the allosteric binding site, since the acetylated analogue is considerably smaller and, thus, loses lipophilic interactions inside the allosteric binding pocket.

**Table 1.** Overview of results from radioligand binding data, calcium mobilization, and receptor endocytosis.

Comp.	Radioligand binding <sup>a)</sup> <i>h</i> CB <sub>2</sub> R: <i>K</i> <sub>i</sub> [nM] (-pIC <sub>50</sub> ± SEM)	Calcium mobilization <sup>b)</sup>		Receptor endocytosis <sup>c)</sup>	
		<i>h</i> CB <sub>2</sub> R pEC <sub>50</sub> (95% CI) [EC <sub>50</sub> , nM]	<i>E</i> <sub>max</sub> ± SEM [%]	<i>h</i> CB <sub>2</sub> R pEC <sub>50</sub> (95% CI) [EC <sub>50</sub> , nM]	<i>E</i> <sub>max</sub> ± SEM [%]
CP55940	13 (7.86 ± 0.15)	7.33 ± 0.10 [46]	96 ± 3	8.40 ± 0.33 [3.9]	95 ± 4
2	15 (7.81 ± 0.12)	7.13 ± 0.09 [75]	101 ± 3	8.68 ± 0.17 [2.1]	99 ± 3
A0	<10% @ 10 μM	nd		nd	
A3	29% @ 10 μM	nd		nd	
A4	4550 (5.32 ± 0.17)	4.94 ± 0.30 [11,400]	76 ± 18	6.17 ± 0.25 [681]	82 ± 5
A5	1950 (5.69 ± 0.19)	na	40 @ 30 μM	na	10 @ 10 μM
B0	36% @ 10 μM	nd		nd	
B2	37% @ 10 μM	nd		nd	
B3	290 (6.52 ± 0.14)	5.65 ± 0.28 [2,720]	149 ± 15	7.44 ± 0.29 [36]	94 ± 4
B4	1520 (5.80 ± 0.21)	5.43 ± 0.26 [3,730]	134 ± 14	7.33 ± 0.17 [47]	88 ± 2
B4o	36% @ 10 μM	nd		nd	
B4m	248 (6.59 ± 0.14)	5.64 ± 0.07 [2,320]	119 ± 4	7.04 ± 0.18 [92]	89 ± 3
B4Ac	36% @ 10 μM	nd		nd	
B5	9050 (5.02 ± 0.27)	5.34 ± 0.17 [4,620]	128 ± 10	7.10 ± 0.26 [79]	91 ± 4

<sup>a)</sup> Performed on CB<sub>2</sub> membranes harvested from stably transfected *h*CB<sub>2</sub>R-HEK cells; <sup>b)</sup> Performed on CHO-K1 cells stably expressing G<sub>αq16</sub> with *h*CB<sub>2</sub>R and the calcium indicator Fura-2-AM; <sup>c)</sup> Performed on FLAG-epitope-tagged CB<sub>2</sub>R stably expressed HEK 293 cells, detected by fluorescently conjugated M1-anti-Flag antibody. nd = not determined, na = not active.

### 2.3. *h*CB<sub>2</sub>R Calcium Mobilization

To further evaluate the pharmacological profile of the synthesized ligands, compounds with >50% binding to CB<sub>2</sub>R (@ 10 μM) were characterized in an intracellular fluorescent calcium mobilization assay to assess G protein-dependent signaling. These studies were performed with *h*CB<sub>2</sub>R overexpressing G<sub>αq16</sub>-coupled CHO-K1 cells using the membrane permeable calcium indicator Fura 2-AM (4 μM). Compound 2 was used as reference compound, as it shows the same range of efficacy and affinity as the high affinity ligand CP55940. Also, the effect of the vehicle (containing <0.5% DMSO) was examined, which did not induce calcium mobilization even at the highest concentration (Figure S1, Supporting Information). In most cases the results of calcium mobilization go in hand with radioligand binding data. Compound A4 shows partial agonism with an *E*<sub>max</sub> = 76% (at 30 μM) and an EC<sub>50</sub> value of 11.4 μM. Surprisingly, A5 only showed an effect on calcium mobilization at the highest concentration (40% at 30 μM), although the compound has a comparable affinity for the CB<sub>2</sub>R as compound A4 (Figure 4A).

Compounds B3–B5 have comparable EC<sub>50</sub>-values in the 1-digit micromolar range (Table 1), and all show *E*<sub>max</sub> > 100% compared to the reference agonist 2 (Figure 4C) in this assay. The B4-derivative with *meta* substitution (B4m) also exhibits more pronounced agonist behavior (“superagonism” compared to the full-agonist reference ligand) with a higher affinity than B4, which is well in line with the results obtained in radioligand binding studies. As an effect of vehicle on calcium mobilization could previously be excluded and artificial enhancement of efficacies could be ruled out, the observed reproducible high extent of efficacy seems to be characteristic for active set B ligands.

### 2.4. Receptor Endocytosis

In the next step, active compounds were analyzed in a CB<sub>2</sub>R internalization assay which requires expression of the β-arrestins (βArr2) pathway (Figure S2, Supporting Information).<sup>[15]</sup> Efficacy of the potentially dualsteric ligands was evaluated regarding their effect on βArr2 mediated endocytosis of FLAG-epitope-tagged CB<sub>2</sub>R stably expressed in HEK 293 cells, detected by fluorescently conjugated M1-anti-Flag antibody and monitored by flow cytometry.<sup>[16]</sup> Agonist response was expressed as percentage of CP55940-mediated internalization at 1 μM. The parent compound 2 proved to be a full agonist in endocytosis with nanomolar potency of EC<sub>50</sub> = 2.1 nM, which corresponds to the value reported in literature.<sup>[10]</sup> The tested potential dualsteric ligands show similar behavior compared to the G protein signaling pathway but with left shifted EC<sub>50</sub>-values (Table 1). Compound A4 again shows partial agonism with *E*<sub>max</sub> = 82%, whereas A5 is not active (*E*<sub>max</sub> = 10% at 10 μM) (Figure 4B). For the compounds of set B, no super-agonism was observed in this assay, and the *E*<sub>max</sub> values are slightly lower than for the parent agonist (Figure 4D). All tested compounds have EC<sub>50</sub> values in a two-digit nanomolar range with the lowest value for compound B3 (EC<sub>50</sub> = 36 nM). Interestingly, among set B compounds, ligand B4m shows the lowest potency (EC<sub>50</sub> = 92 nM), in contrast to the results obtained in G protein signaling.

### 2.5. BRET Interaction Studies

Selected compounds (A4, B3, and B4m) were tested on HEK293 cells transfected with CB<sub>2</sub>R-Luc (Donor) and either mG<sub>si</sub> or βArr2 (acceptors) to further validate their activity in a different and more direct readout. In contrast to calcium mobilization, for mG<sub>si</sub>

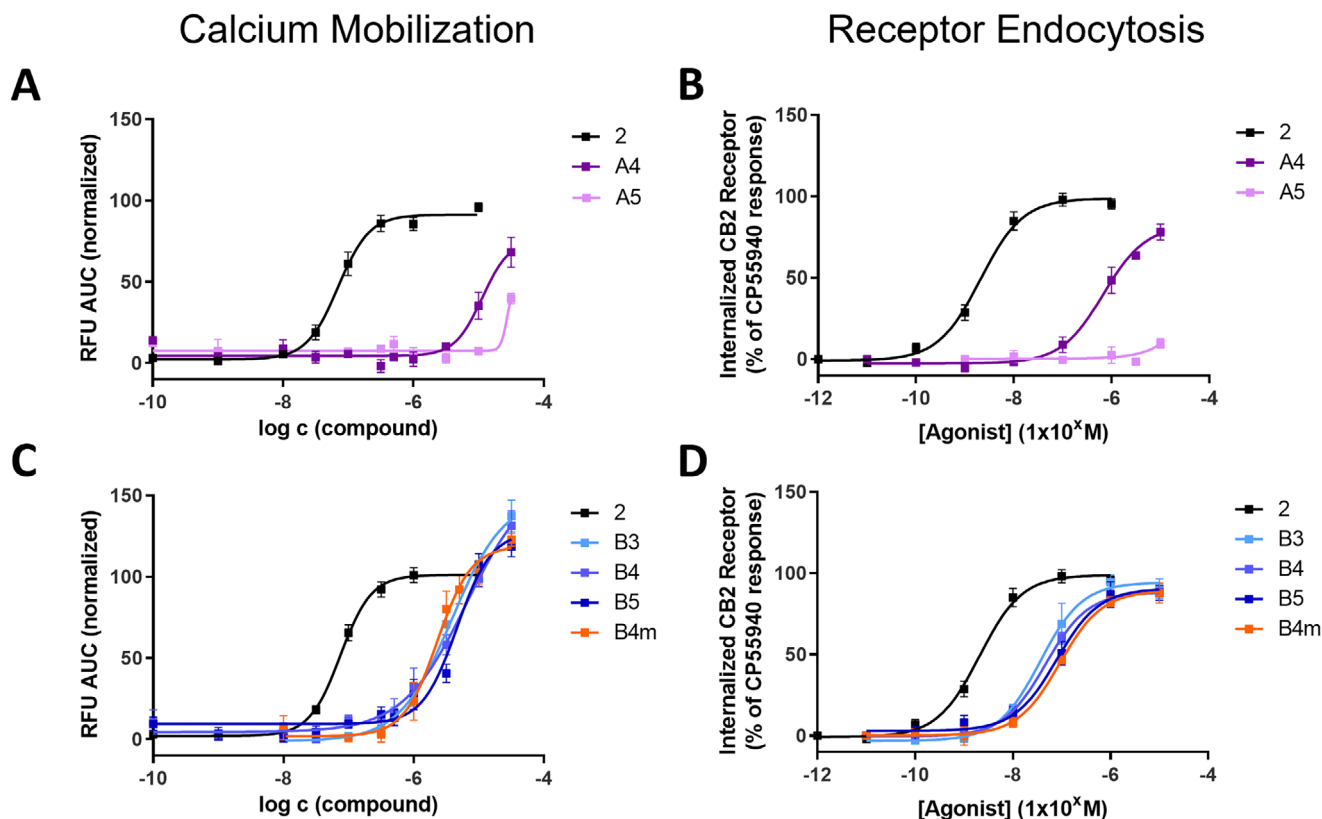


**Figure 4.** Pharmacological evaluation of active compounds. A,C) Calcium mobilization assay; each data-point and error bar represent the average of three independent experiments by duplicate  $\pm$  standard error of the mean (SEM). B,D) Receptor endocytosis; each data-point and error bar represent the average of three independent experiments  $\pm$  standard error of the mean (SEM).

BRET all compounds showed only partial agonism ( $E_{max} = 26\text{--}33\%$ ) compared to CP55940 while the efficacy for  $\beta$ Arr2 recruitment is slightly higher (Figure S3, Supporting Information). Importantly specificity was maintained with none of the compounds demonstrating efficacy at the CB<sub>1</sub>R, despite clear CP55940 responses observed.

## 2.6. Docking Studies

The putative binding mode of the newly developed dualsteric CB<sub>2</sub>R ligands was explored using a docking routine previously optimized by us.<sup>[17]</sup> The ASP<sup>[18]</sup> scoring function available within GOLD<sup>[19]</sup> complemented by DSX\_CSD<sup>[20]</sup> rescoring was found to consistently reproduce the binding pose of the CB<sub>2</sub>R full-agonist WIN 55,212-2<sup>[21]</sup> (PDB ID: 6PT0), with a top-ranked pose which differed by only 0.94 Å from the experimental pose (Figure S4A, Supporting Information). Docking of orthosteric agonist **2** (Figure S4B, Supporting Information)<sup>[10]</sup> suggests a binding mode reminiscent of WIN 55,212-2. The ethoxybenzyl head of agonist **2** occupies the same pocket as the morpholine group of WIN 55,212-2, which is defined by I110, F183, and W194. The benzimidazole core and isopentyl tail of agonist **2** overlap with the heterocyclic core of WIN 55,212-2, thereby keeping the receptor in the active conformation by addressing the “toggle-switch” pair F117 and W258.<sup>[22]</sup> Although the diethylamide tail of agonist **2**

does not completely overlap with the naphthyl tail of WIN 55,212-2, our docking results suggest that agonist **2** establishes similar interactions at the hydrophobic cavity defined by F91, F94, F183, P184, and F281 (Figure S4C,D, Supporting Information). The overlapping interaction networks of WIN 55,212-2 and agonist **2** may account for the potent effect of benzimidazole derivatives as selective CB<sub>2</sub>R agonists reported in the literature.

We proceeded to use our docking routine on the CB<sub>2</sub>R full agonist model to get some structural insights into the full agonist behavior of compound **B3**. Unbiased docking of **B3** yielded a top-ranked pose where the orthosteric portion of the ligand adopts the same orientation as the docking-predicted binding pose for agonist **2** (Figure 5A and Figure S4B, Supporting Information). Additionally, the hydrophobic linker, benzyl ring and 5-bromo-4-methylpyridin-2-one moieties of the positive allosteric modulator portion of **B3** are packed in a manner that adequately addresses the residues of the orthosteric site (highlighted in dark gray in Figure 5). Importantly, the distal cycloheptyl group of **B3** extends beyond the orthosteric site and partially overlaps with the allosteric site proposed by Navarro et al. for some cannabidiol analogs<sup>[23]</sup> (depicted in green in Figure 5B). Our docking results suggest that the cycloheptyl group on **B3** may address the outermost part of the allosteric pocket proposed by Navarro et al., where V36 and A282 are located. Noteworthy, the importance of these two residues for allosteric modulation of CB<sub>2</sub>R has been demonstrated by the authors using mutagenesis studies. This

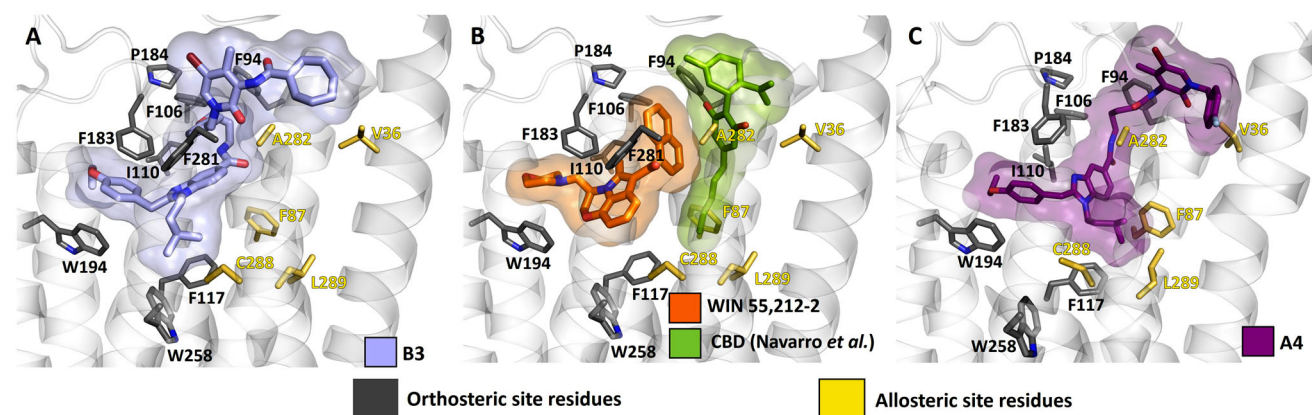


**Figure 5.** A) Predicted docking pose for **B3**, suggesting that the ligand may fully address the orthosteric site of WIN 55,212-2 and partially addresses the allosteric site proposed for CBD. B) CB<sub>2</sub>R model bound to an orthosteric full agonist (WIN 55,212-2, PDB ID:6PT0) superimposed with the CBD allosteric binding mode proposed by Navarro et al.<sup>[23]</sup> C) Docking predicted pose for **A4**, suggesting that the isopentyl tail may be projected toward the proposed NAM hydrophobic cavity defined by F87, C288, and L289. Residues addressed by the orthosteric and allosteric parts are highlighted in black and yellow, respectively.

is consistent with our observation that removal of the cycloheptyl group results in lower receptor affinity for compound **B4Ac** in comparison with **B4**. Additionally, the calculated pose for **B3** suggests that the ligand does not expand toward the intracellular hydrophobic cavity formed by F87, C288, and L289, where the pentyl chain of CBD has been proposed to insert, resulting in its characteristic NAM effect<sup>[23]</sup> (Figure 5B). This is consistent with Navarro's observation that CBD derivatives with shorter aliphatic chains that do not insert into this hydrophobic cavity, tend to behave like PAMs, which might help explain the agonist behavior of series **B**-compounds.

Next, we investigated the hypothesis that the efficacy of compound **A4** is negatively modulated because the molecule occupies the binding position of a NAM. For that, we docked the molecule using the same parameters as for **B3** into the computer model of CB<sub>2</sub>R simultaneously bound to an agonist (JWH-133) and to a NAM (CBD) proposed by Navarro et al. Docking of **A4** produced two top-ranked poses where the ethoxybenzyl head of the agonist portion of the molecule was oriented toward the extracellular loops (DSX\_CSD score  $-180.137$  and  $-179.963$ ). However, these scores were only marginally better than for the third ranked pose (DSX\_CSD score  $-179.012$ ), where the ethoxybenzyl head is correctly oriented toward the intracellular loops, as the docking-predicted binding pose for agonist **2** (Figure 5C and Figure S4B, Supporting Information). Therefore, this pose was selected for analysis. The ethoxybenzyl head of the molecule addresses the hydrophobic cavity defined by I110, F183, and W194, which is experimentally addressed by the morpholine group of WIN 55,212-2,<sup>[21]</sup> and therefore may play a role in the agonistic effect of **A4**. The benzimidazole core and hydrophobic linker engage further interactions with residues involved in WIN 55,212-2 agonism, such as F94, F106, and F117. Importantly, in contrast to the docking results for **B3**, the docking pose for **A4** suggests that the isopentyl tail may be projected toward the intracellular hydrophobic cavity defined by F87, C288, and L289 (Figure 5C). As previously mentioned, this cavity has been proposed to mediate the NAM effect of CBD. Additionally, the distal fluorobenzyl group of **A4** may expand toward the outermost part of the bind-

ing site proposed for CBD by addressing the allosteric residues V36 and A282. All in all, our docking results suggest that **A4** may address residues important for CB<sub>2</sub>R agonism, while simultaneously reaching into the NAM site proposed for CBD. This might help explaining its behavior as partial agonist.

### 3. Conclusions

Our potentially dualsteric ligands described herein were designed by connecting the CB<sub>2</sub>R positive allosteric modulator **1** to the CB<sub>2</sub>R selective orthosteric agonist **2**. The connecting linker was introduced in two different positions of the PAM, explicitly by replacing the cycloheptyl group (set **A**) or by elongation of the benzylic residue (set **B**).

Results of radioligand binding experiments indicate that for set **A** the best spacer length consists of five methylene units, since for the shorter ones affinities drop. For set **B**, the best chain length is represented by three methylene groups. Compounds **B4** and **B5** also fit into the CB<sub>2</sub>R but show lower affinity with increasing linker length. A chain of two carbons is too short for bridging the orthosteric pocket and a nearby allosteric binding site, while substitution in *meta* position of compound **B4** has a comparable effect as shortening the chain-length to compound **B3**. The *ortho* derivative **B4o** on the other hand lost affinity to the receptor as a consequence of the changed orientation of the pharmacophores with respect to each other. By substituting the PAM's cycloheptyl group with a methyl in compound **B4Ac**, we present evidence that activity of set **B** ligands is a result of binding both binding pockets, the orthosteric and a distinct allosteric one. Removing the cycloheptyl group—which is important for positive allosteric modulation<sup>[9]</sup>—leads to less interactions in the allosteric binding pocket and results in lower receptor affinity for compound **B4Ac**, 36% [<sup>3</sup>H]CP55940 displacement at 10  $\mu$ M in comparison to  $K_i = 1.5 \mu$ M for **B4** with total displacement at 10  $\mu$ M. Another method to verify binding would be to selectively mutate a key amino acid in the allosteric pocket and thus uncover the ligands' effects at the mutant receptor.<sup>[24]</sup>



Summing up the results from the efficacy experiments, the two sets show opposite effects. Set **A** compounds exhibit very different behavior within the set with a difference of only one carbon atom in the linker chain making a significant pharmacological difference: three carbon atoms are too short for binding the receptor or bridging both binding sites, while the four-carbon linker compound shows partial agonism. For the largest compound **A5**—which has the best binding value in the set—its efficacy clearly drops. For set **B**, the difference in efficacy is less pronounced for the different linkers. Compounds **B3–B5** show a similar range of efficacy in G protein signaling and  $\beta$ Arr2 recruitment, with  $EC_{50}$ -values slightly better for the smaller compounds. Biased signaling was not further investigated for the  $CB_2R$ -selective molecules as most of the derivatives were comparably active in calcium mobilization and  $\beta$ Arr2 mediated endocytosis. Only compound **B4m** shows—among set **B**—the best  $EC_{50}$ -value in G protein signaling but the lowest in  $\beta$ Arr2 mediated receptor endocytosis. As this compound still exhibits high efficacy in the latter experiment, one cannot speak of bias in this case. Another unusual observation was the excessive calcium release for compounds **B3–B5** and **B4m**, which exceeded the response of the full agonists **2** and CP55940. We could prove that the increased signal at the highest concentration is not caused by the vehicle. Instead, it could be explained by the impact of the positive allosteric modulator incorporated in the ligands. If the allosteric part binds an allosteric pocket, the receptor must be considered as a unique and different system through modulation. Therefore, it is difficult to predict and to compare interactions of an allosteric modulator with different orthosteric ligands, which leads to probe dependence.<sup>[11]</sup>

The drawback which all the herein presented compounds have in common, is the comparatively low receptor affinity in comparison to the orthosteric parent ligand. This might be overcome by further structural optimization through evaluation of the important interactions inside the binding pockets. Still, the ligands show unique signaling profiles different from the compounds' individual components, that is, the ortho- and allosteric ligand, respectively. Moreover, our results provide new insights for the design of dualsteric ligands for this receptor as well as knowledge about the possible topography of associated binding sites.

## 4. Experimental Section

**Chemistry:** All reagents and solvents were directly used as purchased from common commercial suppliers, mainly obtained from SigmaAldrich and BLDPharm. Reactions were monitored by thin-layer chromatography (TLC) with precoated plates with silica gel 60 (Machery-Nagel: ALUGRAM Xtra SIL G/UV<sub>254</sub>). Spots were visualized by UV light (254 and 366 nm). Silica gel 60, 230–400 mesh (Merck) was used for purification by column chromatography. Nuclear magnetic resonance spectroscopy (NMR) <sup>1</sup>H and <sup>13</sup>C spectra were recorded with a Bruker AV-400 NMR instrument (Bruker, Karlsruhe, Germany) in deuterated solvents. Spectra were calibrated with the hydrogen signal of the respective solvent as an internal standard and chemical shifts were expressed in ppm (CDCl<sub>3</sub>: <sup>1</sup>H: 7.26 ppm, <sup>13</sup>C: 77.16 ppm; CD<sub>3</sub>OD: <sup>1</sup>H: 3.31 ppm, <sup>13</sup>C: 49.00 ppm; (CD<sub>3</sub>)<sub>2</sub>SO: <sup>1</sup>H: 2.50 ppm, <sup>13</sup>C: 39.52 ppm). *J* is the coupling constant in hertz (s<sup>-1</sup>). Measurements for verification and purity of the compounds were performed by liquid chromatography mass spectrometry (LC-MS) using a Shimadzu kit, equipped with a DGU-20A3R controller, a DGU-20A degasser, a LC-20AB liquid chromatograph and an SPD-20A UV/Vis de-

tector connected to an LCMS-2020 mass spectrometer (ESI ionization). The stationary phase was a Synergi 4U fusion-RP 80A (150 × 4.6 mm) column, and a MeOH/H<sub>2</sub>O gradient containing 0.1% formic acid was used as the mobile phase. The compounds were dissolved in MeOH and filtered through syringe filters. All target compounds were only characterized further and used for in vitro experiments if a purity of ≥95% was achieved.

**Pharmacology:** The Alexa Fluor 647 Antibody Labeling Kit, as well as Ham's F-12 Nutrient Mix medium (gibco), penicillin/streptomycin, Hygromycin B, Zeocin and Geneticin were obtained from ThermoFisher Scientific (Waltham, MA, USA). Poly-D-lysine and fetal bovine serum (FBS) were obtained from Sigma-Aldrich (Darmstadt, Germany).

**[<sup>3</sup>H]CP55940 Binding Assay:** Radioactive [<sup>3</sup>H]CP55940 was bought from Perkin Elmer LAS (Germany) GmbH. Rimonabant (CB<sub>1</sub>R inverse agonist) and compound **2** were obtained by an in-house synthesis. Saturation and competition binding assays were carried out as previously reported by the authors' group, similar to literature procedures.<sup>[25]</sup> Competition binding experiments were done in 96-well Multiscreen filter plates (Millipore) using seven compound dilutions (0.10 nM–0.32 nM), 0.63 nM [<sup>3</sup>H]CP55940 and membrane homogenate (12.5 μg per well for rCB<sub>1</sub> and 8 μg per well for hCB<sub>2</sub>) diluted in binding buffer (50 mM Tris-HCl; 5 mM MgCl<sub>2</sub>·6 H<sub>2</sub>O; 2.5 mM EDTA; 2 mg mL<sup>-1</sup> BSA, pH = 7.4). After 3 h incubation at room temperature, the reaction was stopped by vacuum filtration and each well was washed with cold binding buffer (4 × 200 μL). Filter plates were dried at 45 °C before IRGA Safe plus-scintillation cocktail (Perkin Elmer) was added (20 μL per well). Activity was counted in a Micro Beta Trilux-Counter (Wallac).

The positive controls, rimonabant, and compound **2**, for CB<sub>1</sub>R and CB<sub>2</sub>R, respectively, were used for normalization of the obtained values for the test compounds. IC<sub>50</sub> values as well as standard errors were determined from sigmoidal dose-response curves applying nonlinear regression and one-side fit logIC<sub>50</sub> as curve fitting functions, using GraphPad Prism 9 software. *K<sub>i</sub>* values were determined according to the Cheng–Prusoff equation:

$$K_i = \frac{IC_{50}}{1 + \frac{[L^*]}{K_D}} \quad (1)$$

*K<sub>i</sub>* values were calculated from at least three individual experiments in triplicate with [L\*] being the radioligand concentration (0.63 nM). *K<sub>D</sub>* values as well as standard errors were determined from homologous binding experiments using CP55940 as hot (radioligand) and unlabeled cold ligand (competitor) and were analyzed from at least three individual experiments in triplicate and were repeated for each new batch of membrane preparation.<sup>[26]</sup>

**Calcium Mobilization Assay:** Chinese hamster ovarian (CHO-K1) cells stably expressing  $G\alpha_{q16}$  with hCB<sub>2</sub>R were cultivated in Ham's nutrient mixture F12 (Merck) supplemented with 10% fetal calf serum and penicillin/streptomycin (90 U mL<sup>-1</sup> / 90 μg mL<sup>-1</sup>). hCB<sub>2</sub> cells were selected using zeocin (200 μg mL<sup>-1</sup>) and hygromycin (200 μg mL<sup>-1</sup>). Cells were plated onto 96-well plates (30,000 cells per well) to a final volume of 100 μL per well and incubated at 37 °C for 24 h. Cells were washed with freshly prepared assay buffer made up from 10 × HBSS (containing final concentrations of 137.0 mM NaCl, 5.4 mM KCl, 1.3 mM CaCl<sub>2</sub>, 0.4 mM MgSO<sub>4</sub>, 0.5 mM MgCl<sub>2</sub>, 0.3 mM Na<sub>2</sub>HPO<sub>4</sub>, 0.4 mM KH<sub>2</sub>PO<sub>4</sub>, 4.2 mM NaHCO<sub>3</sub>, and 5.6 mM D glucose), 1 M HEPES (final concentration 20 mM), bovine serum albumin (1%) and probenecid (dissolved in 1 M NaOH, final concentration 2.7 mM) adjusted to pH 7.4. Cells were loaded with 100 μL Fura-2 AM (4 μM) at 37 °C for 1 h. The dye was removed and 60 μL of assay buffer (100 μL for controls) were added to the dye-loaded cells. Calcium flux was monitored using an automated plate reader (FlexStation 3, Molecular Devices) at an excitation wavelength of 340/380 nm and an emission wavelength of 510 nm. After measuring the baseline for 30 s, test compounds in assay buffer (<0.5% DMSO), compound **2** (positive control) or DMSO (negative control) were added automatically, and fluorescence was monitored for 5 min in total. All experiments were performed in duplicates in at least three independent experiments.  $EC_{50}$  values were analyzed from

the respective area under curve with sigmoidal dose-response curve fitting using GraphPad Prism 9 software.

**CB<sub>2</sub>R Internalization by Flow Cytometry:** The cDNA of the hCB<sub>2</sub>R was a generous gift from Dr Guillermo Yudowski, University of Puerto Rico, and polymerase chain reaction (PCR) was used to amplify the full receptor. PCR was used to delete amino acids 1–25 (as previously described in the literature)<sup>[27]</sup> and create homology sequence with the signal-sequence-Flag vector.<sup>[28]</sup> The final SS-Flag CB<sub>2</sub> receptor were created using NEB-uicler. Stable cell lines were created by transfecting HEK293 cells and selecting with zeocin. Resistant colonies were selected and screened for expression by fluorescent microscopy using anti-Flag M1 (Sigma) conjugated with AlexaFluor-647 (ThermoFisher).

Internalization was measured using a previously described assay.<sup>[16]</sup> Cells were plated in 12-well plates (1 mL per well) two days prior to the assay. The medium was reduced to 500  $\mu$ L per well. Briefly, Flag-tagged hCB<sub>2</sub> receptor was labeled with the calcium sensitive antibody anti-FlagM1 conjugated to AlexaFluor647 at 37 °C for 30 min. Compound dilutions were prepared in DMSO. Cells were incubated with the test compounds for 45 min at 37 °C (containing 0.2% DMSO). Following stimulation, cells were rapidly washed with PBS/EDTA (0.04%) to remove any surface antibody. Cells were suspended in PBS/EDTA (0.04%), pelleted (1200 rpm, 4 °C, 5 min) and resuspended in PBS (containing Ca<sup>2+</sup>) to measure endocytosis. The increase in fluorescence due to previous internalization of the fluorescent tagged receptors was analyzed using a FACSCalibur (BD Biosciences) with 5000 events being analyzed in all cases. The data was analyzed from at least three independent experiments. EC<sub>50</sub> values were analyzed from the normalized response (% of CP55940) with sigmoidal dose-response curve fitting using GraphPad Prism 9 software. For RNAi experiments, 60 mm dishes of CB<sub>2</sub>R HEK293 cells were transfected with 60 pmols of siRNA duplexes from Qiagen (AllStars Negative control, Arrestin 2, Qiagen flexitube Hs\_ARRB1\_11 – CTCGACGTTCT-GCAAGGTCTA, Arrestin 3, Qiagen flexitube Hs\_ARRB2\_10 – CTCGAA-CAAGATGACCAGGTA) using Lipofectamine RNAiMax as per manufactures instructions. Cells were replated into 12 well culture plates and 72 h post-transfection were analyzed for internalization in response to 1  $\mu$ M CP55940 as above. Knockdown was verified by Western Blotting using anti-b-Arrestin 1/2 antibody (CST D24H9 rabbit mAb) (Figure S2, Supporting Information).

**BRET Interaction Studies:** The NLuc8 vector and Venus-mG<sub>si</sub> were gifts from Nevin Lambert (Augusta University) and have been previously described<sup>[29]</sup> and the Arrestin3-YFP was a gift from Meritxel Canals (University of Nottingham).<sup>[30]</sup> The CB<sub>1</sub>R-Luciferase and the CB<sub>2</sub>R-Luciferase was made using the HiFi DNA assembly protocol (NEB) to generate either SS-Flag-CB<sub>1</sub>R<sup>[17]</sup> with CB<sub>1</sub> or SS-Flag-CB<sub>2</sub>R fused in frame at the C-terminus with Renilla Luciferase. HEK293 cells were transfected with CB<sub>2</sub>R-Luc (donor) and either mG<sub>si</sub> or Arrestin 3 (acceptors) at a ratio of 1:4, using PEI (DNA:PEI of 1  $\mu$ g:4  $\mu$ L). 24 h post transfection, cells were reseeded into white 96-well plates and cultured for a further 24 h. On the day of experimentation, the media was replaced with 90  $\mu$ L of Hanks Buffered Saline and equilibrated for 30 min. Cells were incubated for 5 min with 50  $\mu$ M Coelenterazine H (Bioline) for 5 min before addition of 1  $\mu$ L of ligand or DMSO control. 10 min post-stimulation plates were read using a Clariostar plus at 480–20 nm and 530–20 nm. The BRET ratio was determined and expressed as a background corrected (DMSO alone) percentage of that seen for 1  $\mu$ M CP55940.

**Molecular Docking:** The cryo-EM structure of CB<sub>2</sub>R bound to the full-agonist WIN 55,212-2 (PDB ID: 6PT0) and the model of CB<sub>2</sub>R bound to an agonist (JWH-133) and to a NAM (CBD) available a supplementary data of the publication by Navarro et al.,<sup>[23]</sup> were prepared using MOE<sup>[31]</sup> (version 2016.08). MOE's protein structure preparation pipeline<sup>[32]</sup> was used to remove ligands and water molecules, followed by automatic assignment of tautomer and protonation states using Protonate3D<sup>[33]</sup> at pH 7.5. Geometry optimization of WIN 55,212-2, orthosteric agonist **2**, **A4**, and **B3** was performed using the MMFF94x<sup>[34]</sup> force field (gradient convergence criterion: RMS 0.001 · kcal · mol<sup>-1</sup> Å<sup>-1</sup>). The GOLD program<sup>[19]</sup> (v5.4.1) was used to dock the ligands under non-default parameters popsize = 500 and maxops = 500 000. All other parameters were set as default. WIN 55,212-2, orthosteric agonist **2**, and **B3** were docked into the full-

agonist CB<sub>2</sub>R model, while **A4** was docked into the Navarro model. Pose reproduction performance was assessed by RMSD between docked poses and the experimental binding pose of WIN 55,212-2. Using the knowledge-based scoring function ASP1<sup>[18]</sup> for docking, followed by rescoring with the knowledge-based scoring function DSX<sup>[20]</sup> (v0.89), with CSD potentials (version 05/11), was found to robustly model experimentally observed intermolecular interactions of WIN 55,212-2 and to yield a top-ranked pose that differed by 0.94 Å from the experimental pose. 50 poses were computed for each ligand and clustered using fconv<sup>[35]</sup> with an RMSD cutoff of 2.0 Å.

## Supporting Information

Supporting Information is available from the Wiley Online Library or from the author.

## Acknowledgements

This project was financially supported by the German Research Foundation (Deutsche Forschungsgemeinschaft under DFG DE1546/10-1). Gratitude is expressed to the International Doctorate Program “Receptor Dynamics” of the Elite Network of Bavaria (ENB) for financial support of A.T. and S.A.M.S. (grant No. K-BM-2013-247). Y.A.R. was granted a scholarship by the German Academic Exchange Service (Deutscher Akademischer Austauschdienst, DAAD) program “Research stays for university academics and scientists.” D.A.R.-S. was awarded a Ph.D. scholarship by the DAAD. J.N.H. was financially supported by NHS Grampian.

Furthermore, the authors thank Professor Dr. Kristina Lorenz (Institute of Pharmacology and Toxicology, University of Würzburg) for enabling them to conduct in vitro experiments in her laboratory.

Open access funding enabled and organized by Projekt DEAL.

## Conflict of Interest

Y. A. R. is an employee of cannaflos - Gesellschaft für medizinisches Cannabis mbH which has no commercial interests in the results from this work, nor has influenced, determined, or directed the research described in this publication.

## Data Availability Statement

The data that support the findings of this study are available in the supplementary material of this article.

## Keywords

efficacy, G protein-coupled receptor, heterobivalent, positive allosteric modulator

Received: October 12, 2022

Revised: January 30, 2023

Published online:

- [1] L. Matsuda, S. Lolait, M. Brownstein, A. C. Young, T. I. Bonner, *Nature* **1990**, *346*, 561.
- [2] E. Grünblatt, N. Zander, J. Bartl, L. Jie, C.-M. Monoranu, T. Arzberger, R. Ravid, W. Roggendorf, M. Gerlach, P. Riederer, *J. Alzheimer's Dis.* **2007**, *12*, 291.

- [3] a) C. Valant, P. M. Sexton, A. Christopoulos, *Mol. Interv.* **2009**, 9, 125; b) K. Mohr, C. Tränkle, E. Kostenis, E. Barocelli, M. De Amici, U. Holzgrabe, *Br. J. Pharmacol.* **2010**, 159, 997.
- [4] a) T. Kenakin, L. J. Miller, *Pharmacol. Rev.* **2010**, 62, 265; b) L. T. May, K. Leach, P. M. Sexton, A. Christopoulos, *Annu. Rev. Pharmacol. Toxicol.* **2007**, 47, 1.
- [5] G. L. Wenk, *J. Clin. Psychiatry* **2003**, 64, 7.
- [6] a) S. Schramm, L. Agnetta, M. Bermudez, H. Gerwe, M. Irmen, J. Holze, T. Littmann, G. Wolber, C. Tränkle, M. Decker, *ChemMedChem* **2019**, 14, 1349; b) L. Agnetta, M. Bermudez, F. Riefolo, C. Matera, E. Claro, R. Messerer, T. Littmann, G. Wolber, U. Holzgrabe, M. Decker, *J. Med. Chem.* **2019**, 62, 3009; c) L. Agnetta, M. Kauk, M. C. A. Canizal, R. Messerer, U. Holzgrabe, C. Hoffmann, M. Decker, *Angew. Chem. Int. Ed.* **2017**, 56, 7282; d) X. Chen, J. Klöckner, J. Holze, C. Zimmermann, W. K. Seemann, R. Schrage, A. Bock, K. Mohr, C. Tränkle, U. Holzgrabe, M. Decker, *J. Med. Chem.* **2015**, 58, 560
- [7] P. Morales, G. Navarro, M. Gómez-Autet, L. Redondo, J. Fernández-Ruiz, L. Pérez-Benito, A. Cordoní, L. Pardo, R. Franco, N. Jagerovic, *Chem. Eur. J.* **2020**, 26, 15839.
- [8] F. Gado, L. Di Cesare Mannelli, E. Lucarini, S. Bertini, E. Cappelli, M. Digiacomo, L. A. Stevenson, M. Macchia, T. Tuccinardi, C. Ghelardini, R. G. Pertwee, C. Manera, *J. Med. Chem.* **2019**, 62, 276.
- [9] F. Gado, R. Ferrisi, B. Polini, K. A. Mohamed, C. Ricardi, E. Lucarini, S. Carpi, F. Domenichini, L. A. Stevenson, S. Rapposelli, G. Saccomanni, P. Nieri, G. Ortore, R. G. Pertwee, C. Ghelardini, L. Di Cesare Mannelli, G. Chiellini, R. B. Laprairie, C. Manera, *J. Med. Chem.* **2022**, 65, 9918.
- [10] D. Pagé, E. Balaux, L. Boisvert, Z. Liu, C. Milburn, M. Tremblay, Z. Wei, S. Woo, X. Luo, Y.-X. Cheng, H. Yang, S. Srivastava, F. Zhou, W. Brown, M. Tomaszewski, C. Walpole, L. Hodzic, S. St-Onge, C. Godbout, D. Salois, K. Payza, *Bioorg. Med. Chem. Lett.* **2008**, 18, 3695.
- [11] C. Valant, C. C. Felder, P. M. Sexton, A. Christopoulos, *Mol. Pharmacol.* **2012**, 81, 41.
- [12] M. Nimczick, D. Pemp, F. H. Darras, X. Chen, J. Heilmann, M. Decker, *Bioorg. Med. Chem.* **2014**, 22, 3938.
- [13] F. Gado, K. A. Mohamed, S. Meini, R. Ferrisi, S. Bertini, M. Digiacomo, F. D'Andrea, L. A. Stevenson, R. B. Laprairie, R. G. Pertwee, C. Manera, *Eur. J. Med. Chem.* **2021**, 211, 113116.
- [14] a) I. Berque-Bestel, F. Lezoualc'h, R. Jockers, *Curr. Drug Discovery Technol.* **2008**, 5, 312; b) M. Mammen, S.-K. Choi, G. M. Whitesides, *Angew. Chem. Int. Ed.* **1998**, 37, 2754.
- [15] X. Chen, C. Zheng, J. Qian, S. W. Sutton, Z. Wang, J. Lv, C. Liu, N. Zhou, *Curr. Mol. Pharmacol.* **2014**, 7, 67.
- [16] D. Thompson, S. McArthur, J. N. Hislop, R. J. Flower, M. Perretti, *J. Biol. Chem.* **2014**, 289, 36166.
- [17] a) D. A. Rodríguez-Soacha, J. Fender, Y. A. Ramírez, J. A. Collado, E. Muñoz, R. Maitra, C. Sotriffer, K. Lorenz, M. Decker, *ACS Chem. Neurosci.* **2021**, 12, 1632; b) D. A. Rodríguez-Soacha, S. A. M. Steinmüller, A. İşbilir, J. Fender, M. H. Deventer, Y. A. Ramírez, A. Tutov, C. Sotriffer, C. P. Stove, K. Lorenz, M. J. Lohse, J. N. Hislop, M. Decker, *ACS Chem. Neurosci.* **2022**, 13, 2410.
- [18] W. T. Mooij, M. L. Verdonk, *Proteins* **2005**, 61, 272.
- [19] a) J. Cole, J. W. M. Nissink, R. Taylor, *Protein-Ligand Docking Virtual Screening with GOLD*, CRC Press, Boca Raton, FL **2005**. <https://doi.org/10.1201/9781420028775.ch15>; b) M. L. Verdonk, J. C. Cole, M. J. Hartshorn, C. W. Murray, R. D. Taylor, *Proteins* **2003**, 52, 609.
- [20] G. Neudert, G. Klebe, *J. Chem. Inf. Model.* **2011**, 51, 2731.
- [21] C. Xing, Y. Zhuang, T.-H. Xu, Z. Feng, X. E. Zhou, M. Chen, L. Wang, X. Meng, Y. Xue, J. Wang, H. Liu, T. F. McGuire, G. Zhao, K. Melcher, C. Zhang, H. E. Xu, X.-Q. Xie, *Cell* **2020**, 180, 645.
- [22] a) T. Hua, X. Li, L. Wu, C. Iliopoulos-Tsoutsouvas, Y. Wang, M. Wu, L. Shen, C. A. Johnston, S. P. Nikas, F. Song, X. Song, S. Yuan, Q. Sun, Y. Wu, S. Jiang, T. W. Grim, O. Benchama, E. L. Stahl, N. Zvonok, S. Zhao, L. M. Bohn, A. Makriyannis, Z. J. Liu, *Cell* **2020**, 180, 655; b) X. Li, T. Hua, K. Vemuri, J.-H. Ho, Y. Wu, L. Wu, P. Popov, O. Benchama, N. Zvonok, K. Locke, L. Qu, G. W. Han, M. R. Iyer, R. Cinar, N. J. Coffey, J. Wang, M. Wu, V. Katritch, S. Zhao, G. Kunos, L. M. Bohn, A. Makriyannis, R. C. Stevens, Z. J. Liu, *Cell* **2019**, 176, 459.
- [23] G. Navarro, A. Gonzalez, A. Sánchez-Morales, N. Casajuana-Martin, M. Gómez-Ventura, A. Cordoní, F. Busqué, R. Alibés, L. Pardo, R. Franco, *J. Med. Chem.* **2021**, 64, 9354.
- [24] J. Antony, K. Kellershohn, M. Mohr-Andrä, A. Kebig, S. Prilla, M. Muth, E. Heller, T. Disingrini, C. Dallanocce, S. Bertoni, J. Schrobang, C. Tränkle, E. Kostenis, A. Christopoulos, H. D. Höltje, E. Barocelli, M. De Amici, U. Holzgrabe, K. Mohr, *FASEB J.* **2009**, 23, 442.
- [25] a) D. Dolles, A. Strasser, H.-J. Wittmann, O. Marinelli, M. Nabissi, R. G. Pertwee, M. Decker, *Adv. Ther.* **2018**, 17, 1700032; b) S. Mukherjee, M. Adams, K. Whiteaker, A. Daza, K. Kage, S. Cassar, M. Meyer, B. B. Yao, *Eur. J. Pharmacol.* **2004**, 505, 1.
- [26] A. DeBlasi, K. O'Reilly, H. J. Motulsky, *Trends Pharmacol. Sci.* **1989**, 10, 227.
- [27] N. A. McDonald, C. M. Henstridge, C. N. Connolly, A. J. Irving, *Mol. Cell. Neurosci.* **2007**, 35, 237.
- [28] D. Zenko, D. Thompson, J. N. Hislop, *Neuropharmacology* **2020**, 162, 107828.
- [29] Q. Wan, N. Okashah, A. Inoue, R. Nehmé, B. Carpenter, C. G. Tate, N. A. Lambert, *J. Biol. Chem.* **2018**, 293, 7466.
- [30] H. R. Yeatman, J. R. Lane, K. H. C. Choy, N. A. Lambert, P. M. Sexton, A. Christopoulos, M. Canals, *J. Biol. Chem.* **2014**, 289, 15856.
- [31] Chemical Computing Group ULC, *Molecular Operating Environment, Integrated Computer-Aided Molecular Design Platform*, C.C.G., Montreal, QC **2016**.
- [32] a) D. Bashford, K. Gerwert, *J. Mol. Biol.* **1992**, 224, 473; b) P. Labute, *J. Comput. Chem.* **2008**, 29, 1693; c) L. L. Looger, H. W. Hellinga, *J. Mol. Biol.* **2001**, 307, 429; d) J. Desmet, J. Spriet, I. Lasters, *Proteins* **2002**, 48, 31; e) M. K. Gilson, *Proteins* **1993**, 15, 266; f) J. M. Word, S. C. Lovell, J. S. Richardson, D. C. Richardson, *J. Mol. Biol.* **1999**, 285, 1735.
- [33] P. Labute, *Proteins* **2008**, 75, 187.
- [34] a) T. A. Halgren, *J. Comput. Chem.* **1996**, 17, 490; b) T. A. Halgren, *J. Comput. Chem.* **1999**, 20, 730.
- [35] G. Neudert, G. Klebe, *Bioinformatics* **2011**, 27, 1021.